Inelastic neutron scattering studies of defect modes of H in D_2O ice Ih

1994 J. Phys.: Condens. Matter 6 10823

(http://iopscience.iop.org/0953-8984/6/49/023)

J. Phys.: Condens. Matter 6 (1994) 10823–10837. Printed in the UK

Inelastic neutron scattering studies of defect modes of H in D_2O ice Ih

J-C Li†‡ and D K Ross†

† Department of Physics, University of Salford, Salford M6 4WT, UK

‡ Daresbury Laboratory, Warrington WA4 4AD, UK

Received 31 January 1994, in final form 19 September 1994

Abstract. The lattice dynamics of ice Ih (H_2O, D_2O and HDO) have been investigated using inelastic incoherent neutron scattering in the energy transfer range 2–500 meV (i.e. 16–4025 cm^{-1}) using TFXA and HET on ISIS. The spectra of D_2O containing different concentrations of H_2O from 0.5% to 30% by weight were measured. Three main peaks at ~ 105, ~ 185 and ~ 408 meV associated with three localized modes, μ_1, μ_2 and μ_3, of the H defect centre have been observed in the neutron spectra. Two Gaussian components can be resolved in the μ_1 mode, at 103 ± 0.5 meV and 107 ± 0.5 meV, indicating the existence of two different force constants for the H bonds. A lattice dynamical calculation for the H defect in a D_2O ice Ih host lattice, based on our two H bond force constants model, shows the three modes in very similar positions to those observed in the measured data and, in particular, predicts the splitting of the μ_1 peak into modes at 103 and 107 meV.

1. Introduction

When a single defect is introduced into a solid, the dynamics of the defect will differ significantly from the host lattice. For a light defect (or weakly bonded one) there will be localized defect modes which have resonance frequencies that can be distinguished from the phonon modes of the perfect crystal. The majority of the motion of the defect will appear on the atom itself, but the surrounding lattice atoms will respond to a small extent—a response that decays strongly as one moves away from the defect atom. The theoretical analysis of the phenomenon involves the Green's Function [1, 2]. It requires a lattice dynamical model of the unperturbed lattice, and yields the defect mode frequencies and the displacements of all the atoms involved and can be generalized to include charged defects in transparent crystals (F centres etc). These modes can easily be observed in neutron inelastic scattering experiments. The potential advantage of measuring the local mode frequencies due to an isotopic defect is that these frequencies are easier to interpret than are the frequency distributions seen in the bulk modes, which are broadened by dispersive effects. The analysis of defect modes will depend on the nature of the interactions with the neighbouring atoms and hence the measured frequencies will give direct information on these interactions.

Studies of the defect modes due to H in D_2O ice (or D in H_2O ice) have been carried out for many years using Raman and Infrared (IR) techniques [3–7]. High quality IR and Raman spectra have been published and the characteristics of the spectral patterns are well known in the frequency region above 3000 cm^{-1}. The interpretation of these spectra is still unresolved. The assignment made by Whalley [8] based on the view that the intermolecular coupling forces, caused by hydrogen bonding and by the polarization field, give rise to

0953-8984/94/4910823+15$19.50

the collective oscillations, ν_1 and ν_3, that dominate the appearance of the IR and Raman stretching mode complexes is shown in figure 1. The bending mode, ν_2, is determined by the H–O–H bending force constant. The H defect modes in D_2O ice, unlike the stretching and bending modes in the lattice, are decoupled from their surroundings and oscillate with three degrees of freedom while the surrounding atoms are effectively stationary. Here, the assignment of the modes μ_1, μ_2 and μ_3 is also as indicated in figure 1. The orientations of these vibrations have been confirmed by our lattice dynamic calculation. However, for both IR and Raman techniques, because of the selection rules affecting the observed intensity, two of the three defect modes (μ_1 and μ_2) are almost invisible and this makes the interpretation of such spectra difficult. In the past, therefore, more effort has been devoted to studies of the stretching mode, μ_3, and its combination bands. On the other hand, neutron scattering has the very distinct advantage for measurements of H in D_2O, because H has a much larger incoherent cross section than D (its incoherent cross section is some twenty times greater than for D). This, after allowing for the ratio of masses, gives some forty times greater sensitivity for modes involving hydrogen motion as opposed to deuterium. Hence a very small amount of H impurity in D_2O ice can be easily detected. This is dramatically evident in our H contaminated D_2O samples [9]. Clearly H contamination becomes very important for inelastic incoherent neutron scattering for non-hydrogenous samples.

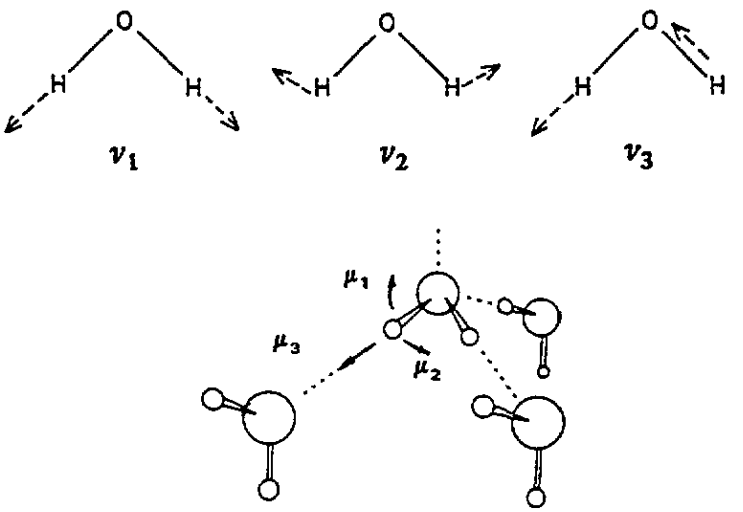

Figure 1. Schematic illustration of the bending and stretching modes, ν_1, ν_2 and ν_3 and the three defect modes, μ_1, μ_2 and μ_3 in ice Ih.

The fundamental importance of studies of the impurity vibrations is that the H atoms, mainly present as HDO molecules, will be bonded just as for D in D_2O ice, apart from possible anharmonicity in the ground state frequencies. The translational symmetry is, however, broken by the H atoms. Hence these atoms will vibrate with three strongly localized modes, μ_1, μ_2 and μ_3 as shown in figure 1. The lowest frequency, μ_1, of HOD ($\sim$ 105 meV) has not been seen so clearly in Raman and IR spectra before and is mainly determined by the H bond force constant. Hence it provides an important test of our lattice dynamic model first proposed in 1989 [10]. The other two modes are located at about 185 and 408 meV. They are located in similar positions to the bending and stretching modes of

H_2O ice Ih and are determined by the bending and stretching force constant respectively. By fitting these modes in our lattice dynamical model, we are thus able to determine the intermolecular and intramolecular force constants.

2. Experimental details

A series of experiments were carried out using the TFXA (time-focusing x-stal analyser) and HET (high-energy transfer) spectrometers on the ISIS pulsed neutron source at the Rutherford Appleton Laboratory [11]. On TFXA, the use of time and energy focusing in conjunction with a pyrolytic graphite analyser in indirect geometry, enables us to make inelastic incoherent neutron scattering (IINS) measurements down to very low energy transfers of ~ 2 meV (in the far-infrared region) with a resolution of $\sim 1\%$ ($\Delta E/E_i$). However, because of the low final analyser energy (~ 4 meV) used, the wavevector transfer Q, increases approximately as the square root of the energy transfer $\hbar\omega = E_i - E_f \simeq E_i$, i.e. $Q \propto \sqrt{\hbar\omega}$ where E_i and E_f are incident and final energies. As the coherent scattering from the H_2O molecule can be neglected, the scattering intensity observed from the sample is proportional to the double differential incoherent cross section per unit neutron energy loss which can be written

$$\frac{d^2\sigma^{inc}}{d\omega\, d\Omega} = \left(\frac{E_f}{E_i}\right)^{1/2} (\langle n(\omega)\rangle_T + 1)\frac{\hbar}{2\omega} G(\omega)$$

where

$$G(\omega) = \Sigma_i(\sigma^{inc}/4\pi)\Sigma_s(C_i^s * Q)^2 \exp(-\langle C_i^2\rangle Q^2)/(3N/\omega m_i).$$

In these equations, $\langle n(\omega)\rangle_T$ is the average occupation number at temperature T for the phonon mode of frequency ω, σ^{inc} is the incoherent scattering cross section of the molecule, $\omega^s(q)$ is the phonon frequency in the sth mode for a wavevector q and $C_i^s(q)$ is the associated eigenvector on the ith atom in the unit cell. These quantities can be evaluated using our version of the lattice dynamics program PHONON at specified values of q for set of assumed force constants. The resulting form of $G(\omega)$ can be obtained by integration over all the possible values of the wavevector q lying in the first Brillouin zone of the crystal. At large Q, the fundamental excitations of the higher energy intramolecular bending and stretching modes of the ice molecule will become submerged in the multiphonon background due to the large Debye–Waller factor, $\exp[-\langle C_i^2\rangle Q^2]$. Hence the HET chopper spectrometer has also been used because it employs large incident and scattering energies, and hence the measurements can be made at low Q values. With this spectrometer, the incident neutron energy is fixed using a rapidly rotating slit package and the energy transfer is obtained by measuring the total time-of-flight of individual neutrons from the sample to the detectors. The resolution is about 1% over an effective incident energy range of 20–2000 meV, depending on which slit package is used. The detectors are all ^{3}He tubes mounted in two banks at 4 m (angles from 3° to 7°) and at 2.5 m (angles from 10° to 30°) from the sample position. This gives HET a background to signal ratio that is negligible for strongly scattering samples such as ice. Thus HET enables us to measure the higher energy transfers at low Q. This is particularly valuable in solids such as ice where the intermolecular bonding is much weaker than the intramolecular bonding, so that the fundamental modes have little dispersion and hence at low Q can be easily separated from the multiphonon and multiple scattering contributions.

3. Single crystal D_2O ice Ih in the energy range from 2 to 150 meV

The single crystal D_2O ice Ih samples were produced in the ice laboratory in the University of Birmingham. Large cylindrical single crystals of ice Ih with a length of 80 mm and a diameter in the region of 45 mm were grown at a rate of about 1 cm per day (for further details, see Ohtomo *et al* [12]). Because of the very low final energy used on TFXA, Q is almost parallel to the incident beam direction. This allows us, to a good approximation, to measure the scattering from single crystal ice Ih both parallel and normal to the c directions for all optic modes at energy transfers above 20 meV. The spectra from single crystal D_2O ice Ih with the Q vector lying approximately (a) parallel to c, and (b) perpendicular to c are plotted together in figure 2. For the D_2O single crystal, this comparison is complicated because the scattering from D_2O is predominantly coherent. Any observed directional dependence of the spectra for the D_2O crystal may be due to dynamical structure factor effects giving extra coherent contributions, and these are difficult to separate from the IINS contribution. Thus, firstly, unlike H_2O, a significant difference was found for the acoustic modes in the energy transfer range 2–15 meV, the spectrum for Q normal to the c axis being much broader than that for Q parallel to the c axis. Secondly, the intensity of the peak at 28 meV for the spectrum with Q parallel to the c axis is stronger than that with Q normal to the c axis. This was not seen in the previous measurement for the H_2O sample [13]. For the librational bands from 70 to 120 meV, the two spectra show slight differences which may also be due to the coherent contributions. For even higher energy transfers, a new peak is observed beyond the librational band at ~ 105 meV. As D_2O should show no intensity in this region, we believe that this is actually due to the very small percentage of H impurity contamination (less than 2% H_2O) introduced during the production of the D_2O crystal. Here the Hs act as defects having three distinct modes with frequencies at 105 ± 0.5, 185 ± 2 and 408 ± 1 meV. The last two high frequencies are less clear due to the large Debye–Waller factor. The peak at ~ 105 meV has the same intensity and shape for both crystal orientations, which suggests that the vibrations have no orientational preference. However, this small percentage of H impurity will not have any effect on the acoustic and molecular optic modes, i.e. it is not the origin of the differences between the two spectra in these regions. This has been confirmed by measuring a better quality (99.96% purity of D_2O) crystal. Subsequently, a series of different concentrations of H_2O in D_2O ice have been measured on TFXA. However, because of the lack resolution and the large Debye–Waller factor in the higher energy range (< 100 meV), some detail in the spectrum was missing [14]. The HET spectrometer has, therefore been used on these samples.

4. HET measurement of H defects at high-energy transfers

As we see for the spectra from the single-crystal samples (figure 2), the defect modes are not orientationally-dependent. Therefore, the measurements can equally well be made using polycrystalline ice on HET, using different concentrations of H to confirm the identification of the defect modes. These defect modes involve hydrogen only and are localized. Therefore, the intensities of these modes are overwhelmingly incoherent. The Q-dependence of the incoherent scattering is only weighted by $|C_i^s \cdot Q|^2$, where C_i^s is the amplitude of vibration. In order to optimize the resolution for different energy peaks, we have to select different incident energies, $E_i = 170$ and 500 meV which are just above the two energy ranges in which we are interested. Figure 3 shows the spectra measured at $E_i = 170$ meV for several concentrations of H_2O as indicated in the figure. By summing up all the low-angle

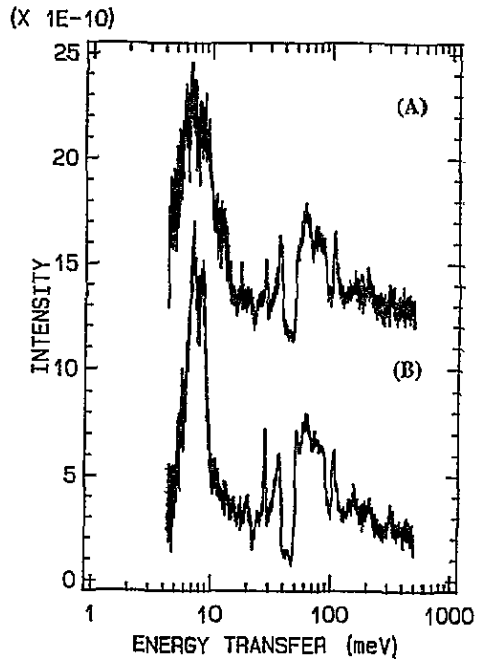

Figure 2. Inelastic incoherent neutron spectra of single crystal D_2O ice Ih measured on TFXA. The upper curve, (A) is the spectrum for Q lying along the c axis of hexagonal ice; the lower curve (B) is the spectrum for Q lying normal to the c axis. The peak at 150 meV is due to contamination by $\sim$ 2% H_2O.

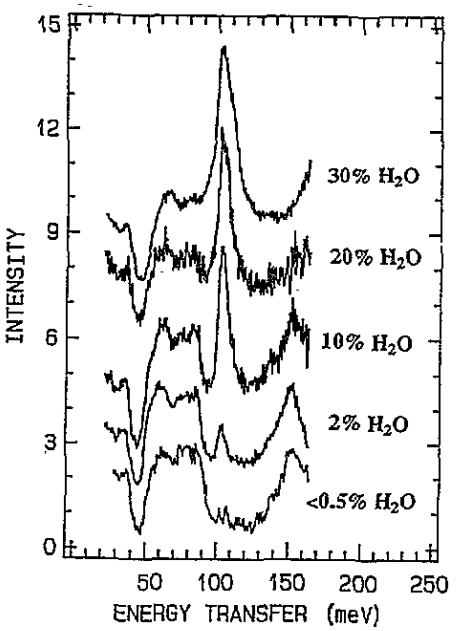

Figure 3. A series of HET measurements (incident energy of 170 meV) for polycrystalline D_2O ice Ih with different concentrations of H_2O. The spectra all show an asymmetrical peak associated with the μ_1 mode at $\sim$ 105 meV, suggesting the presence of two different H-bond strengths.

detectors (4 m bank), the spectra show some details in the μ_1 peak. The spectrum having $< 0.5\%$ H_2O clearly shows two peaks at 103 ± 0.5 and 107 ± 0.5 meV, although these features are only slightly above the statistics with four points on each peak. However, when we closely examine the spectra for higher H_2O concentrations (e.g. 2%, 10%, 20% and 30% H_2O), the peak at $\sim$ 105 meV clearly shows an asymmetrical nature consistent with two components being present. By fitting two Gaussian functions to the peak shape (see figure 4), we were able to determine the separation of the two frequencies and their relative intensities. Details of the fitted parameters are given in table 2. The lower energy component centred at $\sim$ 103 meV has the higher intensity, being about twice as intense as the higher energy component centred at $\sim$ 107 meV. The separation of the two components is about 4 meV. This splitting agrees well with our lattice dynamic calculations, i.e. if the H atom is located on the weak bond, the frequency is lower while if the H atom is located on the strong bond, the frequency is higher (details of this calculation are discussed in the next section). The calculations show flat dispersion curves across the whole BZ for modes involving the protons in the lattice, indicating only weak proton–proton coupling. As the H_2O concentration is increased, the fitting process becomes difficult because other librational modes related to the H_2O molecule begin to emerge under μ_1 and the two modes begin to couple more strongly with each other. Thus it becomes difficult to determine the parameters of the two components. When we examine the spectrum from the higher Q detectors (2 m bank), the data show that the relative intensities of these two components are not changed significantly. This implies that they are all fundamental modes, because the intensities of

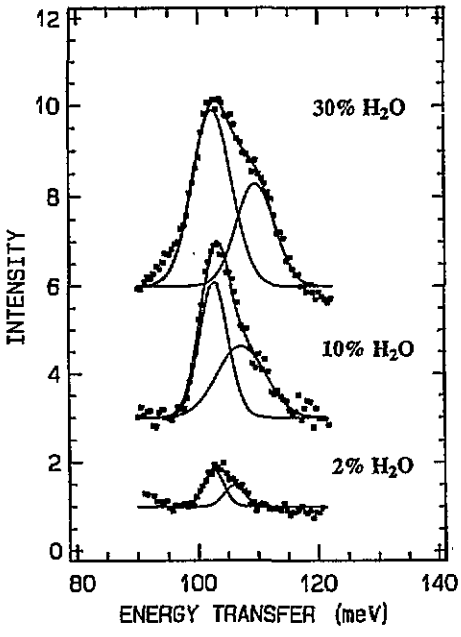

Figure 4. Plot of HET data as in figure 3 in the energy range 90–120 meV, showing two Gaussian functions fitted to the data. The results demonstrate clear evidence for the two components of μ_1, with frequencies at ~ 103 and ~ 107 meV. Parameters as given in table 2 were obtained.

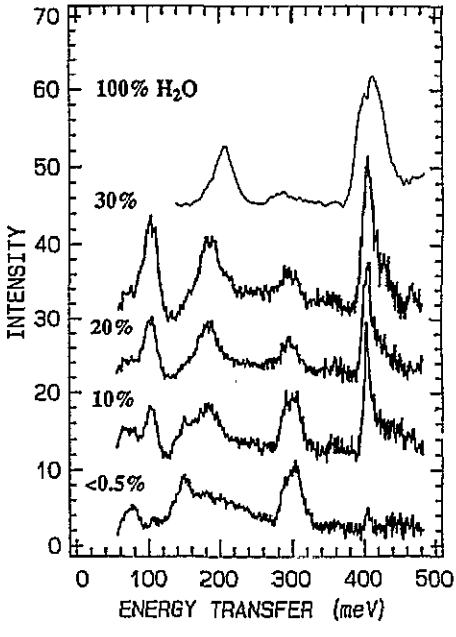

Figure 5. A series of HET measurements on polycrystalline D_2O ice Ih for an incident energy of 500 meV and for different concentrations of H_2O. The spectra all show asymmetrical peaks associated with the μ_2 and μ_3 modes at ~ 185 and ~ 400 meV.

such combinations would vary with $Q^4\exp(-2W(Q))$ rather than $Q^2\exp(-2W(Q))$ for the fundamental modes (where $W(Q)$ is the Debye–Waller factor), i.e. the intensity of the combinations increases more quickly with Q as compared with the normal modes. We can, therefore, rule out the possibility that the splitting is due to any combination bands.

By increasing the incident neutron energy, the detailed structure of the two high-energy modes μ_2 and μ_3 can be seen. The spectrum with 2% H_2O in figure 5 shows no sign of the μ_2 mode. This is not a surprise as the mode will be submerged in the background at that concentration, because the bending mode always shows a very broad and symmetrical hump. For the higher concentration spectra, where the humps are visible, the maxima of the μ_2 peak appear first at 185 meV but are then slightly shifted towards higher energy (by less than 5 meV) as the H_2O concentration is increased. However, it is still a mystery why all H–O–H (or H–O–D) type bending modes are so ill-defined and concentration independent, even though the measurements are always carried out at a very low temperature (20 K), where proton movement (or exchange) should be almost completely eliminated. An analysis of the Q dependence of the intensity indicates that this broad feature is a fundamental mode. However, the position of this peak is considerably lower than the ordinary H–O–H lattice bending modes which appear at 200 meV. Recently, Marechal [15] has been able to observe a very narrow peak in the IR spectrum at 180 meV (1450 cm^{-1}) for HDO in heavy water (10% H_2O) at 300 K using an ATR (attenuated total reflection) technique. This peak is about 18.0 meV (145 cm^{-1}) lower than the bending modes of H_2O, but 21.4 meV (172 cm^{-1}) higher than the similar modes for D_2O, but this author offered no explanation. From the lattice dynamics calculation, we have demonstrated that the isolated H_2O units

Table 1. Comparison of the main features of the vibration spectra of ice Ih, H_2O, D_2O and HDO as observed with INS, IR and Raman techniques: units are meV.

		Neutron						Infra-Red [15]			Raman [16]		
		H_2O	D_2O	2%	5%	10%	30%	H_2O	D_2O	$H(D_2O)$	H_2O	D_2O	$H(D_2O)$
Librational band		70–125	48–89					68–112	53–84		62–118	—	
H-defect mode	μ_1			104	104	104	105			—			—
Bending mode	ν_2	200	152					205	150		205	150	
H-defect mode	μ_2			180	181	182	185			—			—
Stretching mode	ν_1	397	295					400	289		391	291	
H-defect mode	μ_3			408	408	408	408			407			410
Stretching mode	ν_3	414	306					420	308		420	312	

in D_2O lattice should have a much higher frequency (of around 200 meV) than the μ_2 peak, similar to that found in the pure H_2O crystal. In view of the fact that the interactions between water molecules are much weaker than the intramolecular interactions (in the ratio 1:13), the intramolecular frequencies show little dispersion as is confirmed by the phonon calculations. Hence it is not surprising that isolated H_2O molecules have similar H–O–H bending frequencies to the lattice modes of ordinary ice H_2O.

Table 2. Fitting parameters for the peak at $\sim$ 105 meV; $I = A_1 \exp[-W_1^2(E_1 - h\omega)^2] + A_2 \exp[-W_2^2(E_2 - h\omega)^2]$.

		2% H_2O	10% H_2O	30% H_2O
Intensity	A_1	81.7	310.3	426.3
Intensity	A_2	47.4	163.2	219.0
Centre	E_1 (meV)	102.6	102.7	103.5
Centre	E_2 (meV)	106.6	107.3	107.6
Width	W_1 (meV^{-1})	0.171	0.087	0.045
Width	W_2 (meV^{-1})	0.167	0.031	0.043

At even higher energy transfers, the stretching local mode, μ_3 is seen at $\sim$ 400 meV. The peak of this mode is at a similar energy to the stretching lattice modes (ν_1 and ν_3) in the H_2O lattice but is very much narrower. The width of μ_3 is less than 10 meV which is about the resolution of the instrument at this energy. In contrast, the width of the ordinary lattice stretching modes is about 50 meV at this temperature. In fact, the energy position of the μ_3 mode is very similar to the energy position of the ν_1—symmetrical vibrational mode of HOH as shown in figure 1.

5. Lattice dynamical calculation

Lattice dynamical calculations for H defects in ice Ih are relatively easy to understand when a model for ice Ih is established. However, there are many models for the dynamics of ice Ih in the literature [16, 17] and the interpretation of the observed frequency distribution for ice has been a source of controversy for many years. The major difficulty is that, in contrast to the normal phonon density distribution curve for tetrahedral covalent structures, such as Si and Ge, the molecular optic modes in ice Ih are split into two parts. In the hydrogenous form, there is one peak at 28 meV (225 cm^{-1}) and one at 37 meV (298 cm^{-1}). Several possible explanations have been put forward. Renker [18] suggested that the force constants between oxygens parallel and normal to the c-axis of the hexagonal structure are of different strengths. However, this model fails to explain the isotropic nature of the single crystal spectra of ice Ih measured for these directions [13]. Faure and Chosson's [19] suggestion was very similar, namely that there is a partial order of the O–H bonds parallel to the c axis due to long-range forces (without breaking the Bernal–Fowler rules [20]), but no detailed explanation was provided. A more realistic model has been proposed by Wong and Whalley [21]. They suggested that the force constants between oxygens depend on the relative orientations of the two nearest-neighbour water molecules. The differing configurations of the bond asymmetry (see figure 6) cause additional contribution to the force constants. However, the extra contribution from the dipole–dipole (D–D) interactions (or other higher order electrostatic interactions) are too small to cause the large observed separation of the molecular optic modes at 28 and 37 meV. Therefore this idea has not been

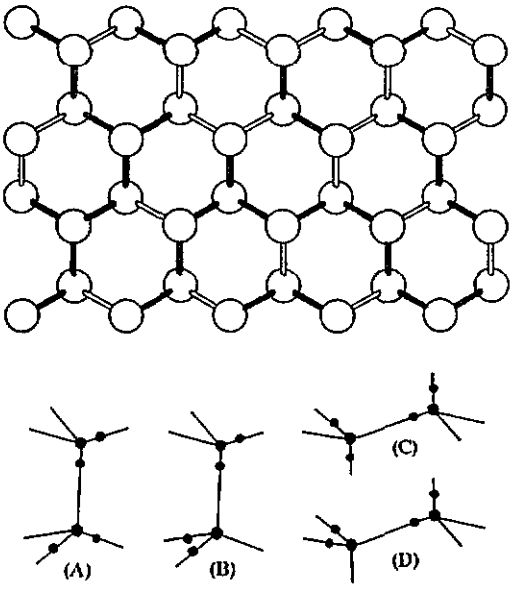

Figure 6. The upper diagram shows a section of the ice I network with a typical arrangement of strong and weak bonds; the strong H-bonds are indicated by the solid bonds and the weak bonds are shown as double lines: the lower diagram shows four possible orientations of molecule pairs in ice Ih. In ice Ic only the (C, strong bond) and (D, weak bond) types of molecule pairs are found.

explored further, although we have adopted the terms 'strong' and 'weak' to correspond to the strong and weak dipole interaction.

In 1978, Klug and Whalley [22] suggested that the two peaks are due to TO and LO splitting, as is seen in ionic crystals, such as NaCl, but gave no detailed theoretical calculation for what the neutron spectrum would look like based on this postulate. Although there were some disagreements as to whether the idea of TO and LO splitting is valid for ice, because the argument for it depends on the existence of strong long-range interaction, it has been accepted generally for the explanation of the weak shoulder at 35 meV in IR and Raman spectra. Lately it has been extended to explain the two molecular optic peaks at 28 and 37 meV seen in IINS spectrum. There are, however, a number of strong arguments against this theory that have emerged as result of our recent measurements on a range of different ice structure using IINS, including all 'recovered' high-pressure phases of ice. These studies show that the two peaks at 28 and 37 meV do not necessarily always appear in the spectrum for different phases of ices.

The general point to be made is that the TO–LO interpretation is based originally on the interpretation of the IR and Raman data where one is emphasizing $q = 0$ behaviour whereas the neutron technique, which shows the splitting much more clearly is a direct measurement of the PDOS over the whole BZ. Therefore, features in the measured PDOS should have a weight proportional to the number of modes associated with that feature, i.e. the TO modes at about 28 meV should have twice the weight of the higher energy modes at about 37 meV, because there are two TO modes for every one LO mode (the ratio is 2:1). Our data for ice Ih and Ic, however, show the opposite ratio (figure 7). This may be the reason that Whalley, Klug and Handa [23] have assigned the molecular optic peak at 28 meV to the LO modes and the peak at 37 meV to the TO modes, which is opposite to the early assignment [22],

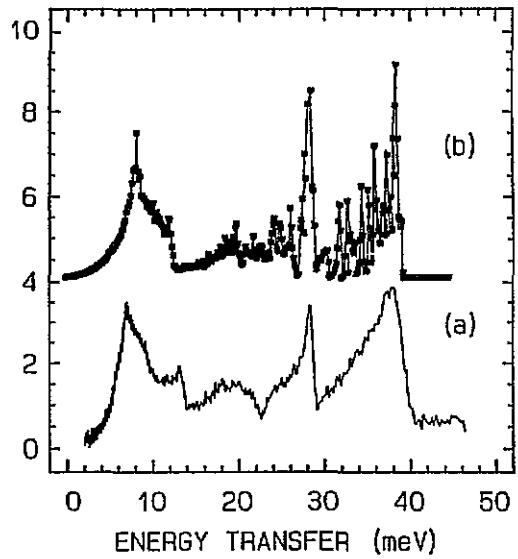

Figure 7. The diagram shows the weighted one-phonon density of states $G(\omega)$; (*b*) is the calculated $G(\omega)$, showing that the two triangular peaks as observed in the measured $G(\omega)$ for H_2O ice, (*a*), are well reproduced. The right-hand diagram shows dispersion curves for ice Ih calculated using the model, which shows two flat regions at 27 and 36 meV, giving the sharp higher energy cut offs.

without giving any explanation of the new assignment.

The second argument against TO and LO splitting is that the same relative intensities of the two peaks do not appear in all phases of ice, i.e. some spectra have only the low-energy peak, e.g. the spectrum for ice VIII, while some spectra have only the high-energy peak, e.g. ice on the surface of porous media. In other cases, the spectra have both peaks, but the relative intensities of these peaks vary from one form of ice to another.

In order to provide an explanation for all the features of these ice spectra, we have to conclude that the two molecular peaks are associated with the different possible dipole–dipole (D–D) configurations as shown in figure 6. The best example is ice VIII. Because the structure of ice VIII is fully ordered (TO and LO splitting is actually more likely to happen in this case), there is only one type of D–D arrangement (*D* in figure 6) in the structure, which is associated with the 'weak' H-bond interaction. That is the reason why the spectrum of ice VIII has the low-energy peak only. At high temperatures (above 0 °C), the protons in ice VIII become disordered, namely ice VII. Because the other type of D–D arrangement, (C in figure 6 associated with the 'strong' H-bond), now also exists due to the proton disordering, the high-energy peak reappears in the spectrum of ice VII [24]. This relationship is also consistent with other forms of ice, such as ice Ih and Ic. We, therefore, believe that the relative intensities of the two optical bands are entirely dependent on the actual ratio of these configurations corresponding respectively to the strong and weak H-bonds in the ice structure. For instance, in ice Ic (which has an identical spectrum to ice Ih), the protons are completely disordered. Hence, statistically, it has one bond with configuration C to two with configuration D. Therefore, in ice Ic, there will be one weak H-bond for every two strong H-bonds (ratio is 1/3:2/3). They are randomly and isotropically distributed in the ice structure which gives the low/high energy peaks in a ratio of 1:2 as observed. Furthermore, the difference between the two H-bond force constants are considerably larger than can

be explained on the basis of electrostatic effects only. A simple calculation using the relationship of $\omega \simeq \sqrt{k/m}$ (where ω is the vibrational frequency and k is the force constant) gives an estimating ratio of the two H-bond force constants as $k_1 : k_2 = (\omega_1 : \omega_2)^2 \simeq 1 : 1.9$ (the exact values are determined though the lattice dynamical calculations). The molecular orbitals, however, are known to be influenced strongly by correlations in the orientation of neighbouring molecules. The actual source of the splitting H-bond, therefore, must lie at the molecular orbital level.

Based on the above background, Li and Ross [25] recently proposed a two H-bond force-constant model for ice. In this model, the randomly oriented configurations of the dipole arrangements cause the optic modes to split into two groups, the separation in energy being proportional to the difference in the strengths of the two force constants arising from the four different types of local molecular arrangements in the hexagonal structure. By adopting empirical values for the two H-bond force constants of 2.1 and 1.1 eV/Å^2, and by then randomly inserting these two values of the H-bond force constant into a large super-lattice (to represent the disordering of the protons) in ratio of 2/3:1/3 (i.e. for every one strong bond in the lattice there are two weak ones), the dispersion curves and the integrated phonon density of states have been calculated [14]. The resulting calculated phonon dispersion curves and densities of states, $G(\omega)$, agree well with the experimental data. Figure 7 shows a typical result for $G(\omega)$. The calculated $G(\omega)$ is based on a large super-lattice model with a random distribution of the strong and weak bonds, the total PDOSs are integrated over all possible modes in the first BZ and weighted by the amplitudes of the vibrational modes. The calculated $G(\omega)$ can only be directly compared with a measured spectrum which is predominantly incoherent scattering. For an H_2O molecule, the total coherent cross section 9.58×10^{-24} cm^2 and total incoherent cross section is 80.3×10^{-24} cm^2.

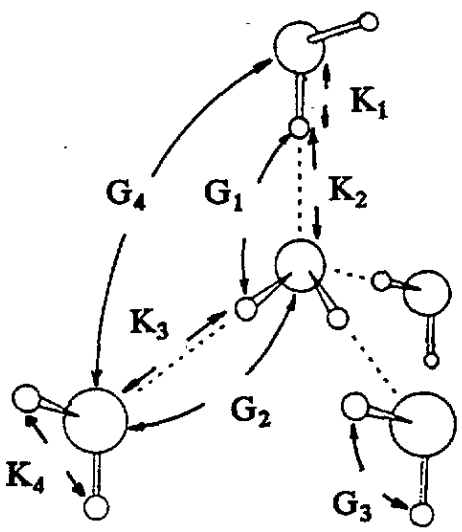

Figure 8. The force constants used in the PHONON calculations.

Using the same model, we are able to estimate the frequencies for the defect modes by introducing a single H atom into the D_2O lattice. Because we are only interested in the three defect modes, the need for a large super-lattice can be avoided by using a single primary unit cell with 4 oxygens (space group considering oxygen atoms only is $P6/mmc$)

Table 3. Force constants for ice Ih used in PHONON calculations and their main effects. Units: stretching force constants, K, are expressed eV $Å^{-2}$, bending force constants, G, in eV Rad^{-2}.

Force constant	*Value*	*Main effect of force constant*
K_1 O–H bonding	35.9	Affects the internal modes.
K_2 strong O···H bonding	2.1	Affects the optic modes in the translational region.
K_3 weak O···H bonding	1.1	Same as for the K_2.
K_4 H···H bonding	−1.2	Separate ν_1 and ν_3.
G_1 H···O-H bending	0.78	Affects the acoustic modes and the width of the librational modes.
G_2 O···H–O bending	0.45	Level of low energy cut-off of the librational band.
G_3 H–O–H bending	3.2	Affects the internal modes.
G_4 O···O···O bending	0.16	Affects the acoustic modes.

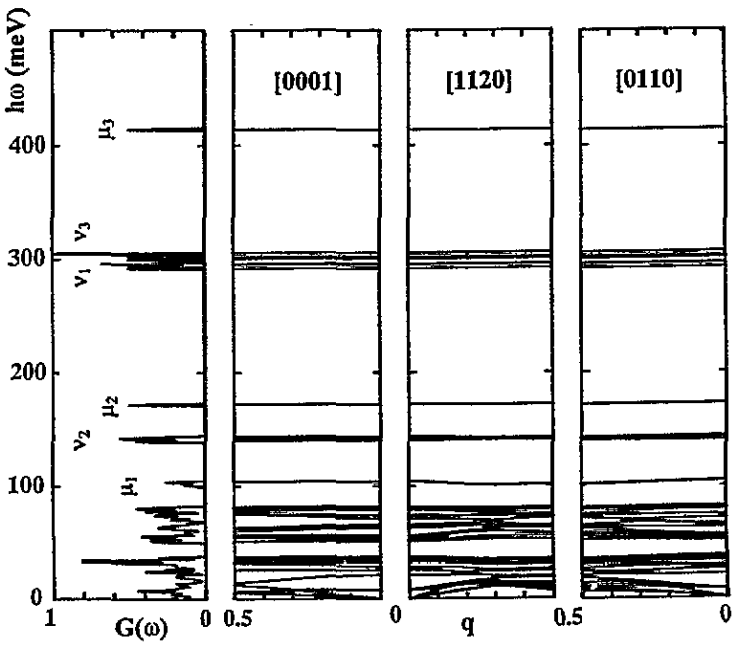

Figure 9. Calculated dispersion curves for one H atom on a strong H-bond. The curve on the left is the integrated phonon density of states for all the three principal symmetry directions. Note that this is not a complete phonon density of states which would require summation over all points in the first Brillouin zone.

and 8 hydrogens. Even though the method employed in the PHONON calculations means that the model is effectively for a periodically repeating proton, these protons couple so weakly with each other (i.e. the corresponding dispersion curves are essentially flat) that the use of the primary cell is still valid. The strong H-bonds (SHB) and the weak H-bonds (WHB) are introduced in an artificial way. Other force constants are taken from the ice Ih model [14] as shown in table 3 and indicated in figure 8. By putting H atoms on different H-bonds, the phonon dispersion curves are calculated across the first BZ as shown in figure 9. Here, the diagram on the left is the density of states. As can be seen, two of the three defect modes, μ_2 and μ_3, at $\sim$ 185 and $\sim$ 400 meV, are very flat and the lowest frequency one (μ_1) at $\sim$ 105 meV has only a slight dispersion. If two H atoms are inserted in the unit cell (equivalent to $1/6 = 16\%$ H_2O concentration), there is little evidence of coupling

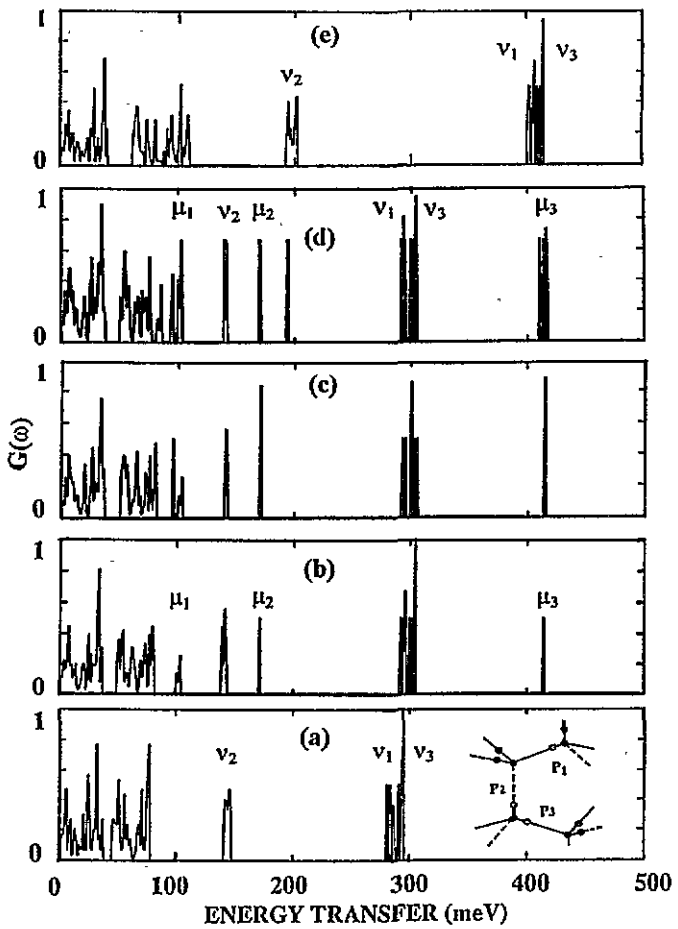

Figure 10. The calculated phonon density of states, $G(\omega)$ for different positions of the H atoms. The inserted sketch shows the possible positions (P_1, P_2 and P_3) of the H-defects. The H atoms are indicated by the open circles and the D are solid circles. The dashed lines indicate the weak H-bonds (K_3). Curve (*a*), for a D_2O lattice without an H-defect; (*b*), an H atom is introduced on the P_1 position (a strong H-bond); (*c*), two H atoms are introduced, one on a strong H-bond (P_1) and another on a weak H-bond (P_2), but on two different water molecules; (*d*), three H atoms are introduced (P_1, P_2 and P_3), two of them on the same water molecule; and (*e*), for a pure H_2O lattice.

between them, i.e. if both H atoms are on SHBs, there are two curves corresponding to the same frequency for the μ_1 mode and similarly if both are on WHBs. If one H is on a SHB and another on a WHB, two branches are produced in the spectrum, having a separation of 4 meV. This is remarkably close to the splitting observed in the IINS spectrum. Figure 10 shows the phonon density of states as shown in the curves on the left-hand side of figure 9.

It is interesting to note that when the two H atoms are on the same water molecule (i.e. HOH), μ_2 has a frequency of 200 meV which is much higher than the μ_2 for an HDO molecule. This implies that the observed peak is due to HDO. Even in the spectra for 30% H_2O, there is still no indication of modes at 200 meV, implying that there are still only very few HOH units. If we assume that the potential wells are harmonic, the total zero

point energy will be less if the H is on the WHB and D is on the SHB. As a result, H atoms prefer to occupy the WHB and hence are unlikely to form HOH molecules, because only 1/3 H-bonds are WHB statistically speaking. Therefore, the probability of forming HOH molecules is reduced significantly. It should be emphasized that this particular situation should occur at very low temperatures (< 120 K) where there is no proton mobility (H and D are all frozen). At higher temperatures, room temperature and above, the very small amount of energy difference between the SHB and WHB is smeared by the thermal agitation energy, so that there may be no such selective behaviour.

On examining the highest frequency defect modes, μ_3, a very narrow peak can be seen with a full width at half height of 10 meV, even when the concentration of H_2O is increased to 30%. From the calculation it is seen that the stretching frequencies are very little affected by whether the bond is a SHB or a WHB. This is easy to understand because the intramolecular force constant is an order of magnitude higher than the intermolecular force constants. However, the width of the intermolecular stretching modes for ordinary ice Ih is more than 50 meV as measured by IR [15], Raman [16] and IINS [14]. The traditional explanation for the broadness of this band is based on anharmonicity [26]. We believe there is a further contribution, namely that the splitting of the H-bond strengths may also affect the nature of the covalent bond, resulting in the spread in the strengths of the covalent bond.

6. Summary

In this paper, we present the first neutron spectroscopic measurements of H-defect modes in ice Ih. Since the sharp peaks for these point defect modes are dynamically decoupled from the lattice modes of neighbouring vibrators, they provide direct information about the interactions of the defects with the other lattice molecules. Hence, even a simplified lattice dynamic model for the environment of a defect in the harmonic approximation can be interpreted unambiguously to yield fundamental information about the H-bond strengths. The Q-independence of the intensity ratio of the two components of the μ_1 peak indicate that these are both fundamental modes and can, therefore, be considered as further evidence for the two strengths H-bond model. The implication of this discovery is of considerable importance for water science as a whole, because it may be responsible for the well-established 'anomalies' of water. Thus the two force constants must be related to two different H-bonding energies, which, in turn, can provide a mechanism and a sensible explanation for the abnormal thermodynamic properties of water. Moreover, if the point defects fall into two categories, according to the bond on which they are located (i.e. on SHB or WHB), these two types of defects will have different activation energies which could be measured by electrical conductivity or by dielectric relaxation.

Acknowledgments

The authors would like to thank the Science and Engineering Research Council (UK) for financial support and the Rutherford Appleton Laboratory for the use of neutron facilities. The authors are also grateful to Dr R W Whitworth, for supplying the single crystal ice Ih and to him and Dr J Glen for useful discussions.

References

[1] Dawber P J and Elliott R J 1964 *Proc. R. Soc.* A **277** 222
[2] Maradudin A A 1985 *Rep. Prog. Phys.* **28** 331
[3] Whalley E and Bertie J E 1967 *J. Chem. Phys.* **46** 1271
[4] Ikawa S-I and Maeda S 1968 *Spectrochim. Acta* A **24** 655
[5] Hobbs P V 1974 *Physics of Ice* (Oxford: Oxford University Press)
[6] Sivakumar T C, Chew H A M and Johari G P 1978 *Nature* **275** 524
[7] Devlin J P 1990 *Intern. Rev. Phys. Chem.* **9** 29
[8] Whalley E 1977 *Can. J. Chem.* **55** 3429
[9] Li J-C and Ross D K 1992 *ISIS Experimental Report*
[10] Li J-C, Ross D K and Hayes M H B 1994 *J. Mol. Struct.* **322** 131
[11] Boland B C 1990 *ISIS Experimental Facilities* Rutherford Appleton Laboratory, UK
[12] Ohtomo M, Ahmad S and Whitworth R W 1987 *J. Physique Coll.* **48** Suppl. No 3 C1–595
[13] Li J-C, Ross D K, Howe L and Tomkinson T 1989 *J. Physica* B **156&157** 376
[14] Li J-C and Ross D K 1992 *Physics and Chemistry of Ice* ed N Maeno and T Hondoh (Hokkaida University Press) p 27
[15] Marechal Y 1991 *J. Chem. Phys.* **95** 5565
[16] Shawyer R E and Dean P 1972 *J. Phys. C: Solid State Phys.* **5** 2028
[17] Scherer J R and Snyder R G 1977 *J. Chem. Phys.* **67** 4794
[18] Renker B 1973 *Physics and Chemistry of Ice* ed E Whalley, S J Hones and L W Gold (Toronto: University of Toronto Press) p 82
[19] Faure P and Chosson A 1971 *Light Scattering in Solids* ed M Balkanski (Paris: Flammarion Sciences) p 272
[20] Bernal J D and Fowler R H 1933 *J. Chem. Phys.* **1** 515
[21] Wong P T T and Whalley E 1976 *J. Chem. Phys.* **65** 829
[22] Klug D D and Whalley E 1978 *J. Glociol.* **85** 55
[23] Whalley E, Klug D D and Handa Y P 1991 *J. Mol. Struct.* **250** 337
[24] Li J-C and Ross D K 1994 *ISIS Annual Experimental Report*
[25] Li J-C and Ross D K 1993 *Nature* **365** 327
[26] Rice S A, Bergren M S, Belch A C and Nielson G 1983 *J. Phys. Chem.* **87** 4295